American Mineralogist, Volume 80, pages 560–575, 1995

Heat capacities and thermodynamic properties of braunite (Mn_7SiO_{12}) and rhodonite ($MnSiO_3$)

RICHARD A. ROBIE, J. STEPHEN HUEBNER, BRUCE S. HEMINGWAY
U.S. Geological Survey, 959 National Center, Reston, Virginia 22092, U.S.A.

ABSTRACT

The heat capacities, C_P^0, of synthetic rhodonite ($MnSiO_3$) and braunite (Mn_7SiO_{12}) have been measured by adiabatic calorimetry from 6 to ~350 K. The heat capacity of braunite was also measured to ~900 K by differential scanning calorimetry. Braunite exhibits a λ-peak (paramagnetic to antiferromagnetic transition) in C_P^0 in the temperature region 93.4–94.2 K. Rhodonite did not show the expected peak in C_P^0 characteristic of the cooperative ordering of the Mn^{2+} spins at temperatures above 6 K.

At 298.15 K the standard molar entropy of rhodonite is 100.5 ± 1.0 and that of braunite is 416.4 ± 0.8 J/(mol·K). For rhodonite, $\Delta_f H^0(MnSiO_3, 298.15\ K)$ is −1321.6 ± 2.0 kJ/mol. For braunite, the value for $\Delta_f H^0(Mn_7SiO_{12}, 298.15\ K)$, −4260 ± 3.0 kJ/mol, was obtained by considering both calorimetric and phase-equilibrium data. Our heat capacity and entropy values were combined with existing thermodynamic data for $MnCO_3$, CO_2, SiO_2, MnO, and Mn_3O_4 in a "third-law" analysis of several phase equilibrium studies and yielded $\Delta_f G^0(MnSiO_3, 298.15\ K) = -1244.7 \pm 2.0$ kJ/mol and $\Delta_f G^0(Mn_7SiO_{12}, 298.15\ K) = -3944.7 \pm 3.8$ kJ/mol from the elements.

A revised petrogenetic grid for the system Mn-Si-O-C at 2000 bars is presented and is consistent with both thermochemical values and occurrence of natural assemblages.

INTRODUCTION

In a general way, the occurrence of Mn^{4+}-bearing minerals reflects the influence of the Earth's atmosphere, and the occurrence of Mn^{2+}-bearing minerals reflects deep crustal processes or the influence of organic C. Most Mn that occurs naturally reflects, both volumetrically and by number of species, one or the other of these two oxidation states. Of the Mn-rich minerals in which the Mn is generally divalent, rhodonite and its polymorph, pyroxmangite (for which rhodonite can be easily mistaken), are the most abundant silicates and are exceeded in abundance only by rhodochrosite, $MnCO_3$. Natural Mn^{3+}-minerals are uncommon. Of the naturally occurring manganese oxides, carbonates, and silicates, only five silicates (manansilite, piemontite, kanonaite, macfallite, and okhotskite), members of the braunite group (braunite, braunite-II, neltnerite, and abswurmbachite), bixbyite, and hausmannite contain Mn^{3+} as an essential constituent. Thus, there are relatively few Mn-rich minerals that contain Mn^{3+}, which might reflect environments where atmospheric and crustal processes interact. Braunite is the most common of these 11 phases.

Accurate thermochemical data for rhodonite and braunite are desirable for a number of reasons. First, because braunite is one of the few minerals that reflects conditions of the interface between the crust and the atmosphere or hydrosphere, knowledge of braunite equilibria can help improve the deduction of regional metamorphic conditions, particularly those at relatively high f_{O_2}. Second, braunite occurs in zones that have been subjected to intense postdepositional soft-sediment and tectonic deformation, resulting in broken or dismembered rock units that are no longer in horizontal or vertical stratigraphic continuity, and the occurrence of this distinctive mineral may prove to be a valuable indicator of paleoconditions and, thus, paleoenvironments with intermediate oxidation states, such as the ocean floors. Finally, knowledge of braunite phase equilibria may improve the extractive metallurgy of Mn. Similar arguments can be made for studying rhodonite, although rhodonite is not as significant as braunite for deducing inherited high f_{O_2} values.

OCCURRENCE

Braunite is both an ore-forming mineral and a precursor of supergene (quadrivalent) oxide ores in stratabound Mn deposits worldwide. Examples of economically important deposits include the extensive, unmetamorphosed Mamatwan-type ores of the Hotazel Formation, Kalahari Basin, South Africa (Nel et al., 1986; Miyano and Beukes, 1987) and the metamorphosed Sausar Group, India (Roy et al., 1986). Small braunite-bearing lenses, enclosed by rhythmically interbedded chert and shale, are common in tectonically active (and biologically productive) zones thought to be related to midocean-ridge hydrothermal activity (Bonatti et al., 1976; Crerar et al., 1982) and to diagenesis within continental margin sediments (Hein et al., 1987). Huebner et al. (1992) suggest

0003–004X/95/0506–0560$02.00

that some such deposits might have been precipitated at the seafloor where relatively reducing, subseafloor fluids mixed with fresh seawater.

The ultimately sedimentary origin of most braunite is best revealed by its occurrence in Mn-rich lithologies that have been altered by little more than diagenetic processes (Nel et al., 1986). Huebner and Flohr (1990) suggest that some braunite layers were formed as a gel-like precipitate. Ostwald and Bolton (1990) describe braunite concretions of diagenetic origin within shales in Western Australia.

Knowledge of the mineral assemblages in which braunite occurs will prove useful in constructing the Mn-Si-C-O petrogenetic grid, particularly in positioning equilibria with large uncertainties in the $\Delta_r G$. Braunite assemblages are found in rocks of all metamorphic grades. Roy (1965), Dasgupta and Manickavasagam (1981), and Dasgupta et al. (1990) summarized mineral assemblages or associations. The critical assemblages involving braunite range from pyrolusite + braunite + quartz at greenschist grade; pyrolusite + braunite + quartz and braunite + bixbyite + quartz at biotite grade; braunite + rhodonite + quartz at garnet and staurolite-kyanite grades; and braunite + bixbyite + quartz and braunite + rhodonite + quartz at sillimanite grade. Progressively higher temperatures resulted in braunite coexisting with more reduced manganese oxides and ultimately with rhodonite or pyroxmangite. A proven assemblage involving braunite and tephroite in nature is not known to us, but we note a report of hausmannite + braunite + tephroite of unknown composition and textural relationship (Abs-Wurmbach et al., 1983). Huebner (1967, 1969) suggested that steep f_{O_2} gradients must have existed between these braunite-bearing assemblages and surrounding Mn-poor, Fe^{2+}-rich country rocks: the braunite-bearing assemblages had the capacity to maintain, and the ability to record, the relatively high O potentials of the sedimentary environments in which the Mn was originally deposited. Subsequently, Dasgupta et al. (1985) confirmed the hypothesis.

Rhodonite and pyroxmangite are pink to red and easily noticed; for this reason, there are many reported occurrences. Most rhodonite appears to form in one of three environments: hydrothermal, pegmatitic, and (regional or contact) metamorphic. Volumetrically, the most important occurrences are found in hydrothermal (where the manganese silicate forms a gangue) and regional metamorphic environments. These rhodonite-forming environments lie beneath the surface of the Earth's crust; the occurrence and preservation of rhodonite records a continuous history of low to moderate oxidation state. If exposed to atmospheric weathering processes, the manganese silicate rapidly transforms to quadrivalent oxide.

In regional terranes, the metamorphic grade at which rhodonite appears depends upon the bulk composition or mineral assemblage. In Mn-oxide-rich metasediments (assemblages containing pyrolusite, bixbyite, braunite, hausmannite, or vredenburgite), rhodonite is absent in greenschist and biotite grades but common in garnet and higher grades (see Dasgupta and Manickavasagam, 1981). In the absence of manganese oxides, rhodonite and pyroxmangite occur at greenschist facies (Peters et al., 1973; Abrecht, 1989). [Flohr and Huebner (1992) described a zeolite-facies deposit in which rhodonite and hausmannite occur but never in the same assemblage.] Thus, it would appear that rhodonite and braunite occur in equilibrium only at relatively high temperatures, >675 K.

Huebner (1967) noted that at low metamorphic grades rhodochrosite ($MnCO_3$) can occur with either braunite or rhodonite, but not both phases. He presented evidence that at relatively low f_{O_2} and temperature, the assemblage $MnCO_3 + SiO_2$ reacts to rhodonite + CO_2. Although braunite and rhodochrosite coexist in apparent equilibrium (Huebner and Flohr, 1990), no direct evidence for a comparable reaction, rhodochrosite + quartz + O_2 = braunite + CO_2, is known to us. Nevertheless, given appropriate bulk compositions, it is clear that rhodochrosite + quartz is a low-temperature assemblage relative to assemblages that contain rhodonite, and a low f_{O_2} assemblage relative to assemblages that contain braunite.

Crystal chemistry and phase equilibria of rhodonite and braunite

The mineralogical end-member composition of rhodonite is $CaMn_4Si_5O_{15}$, but the solid-solution range of the rhodonite structure extends to $MnSiO_3$, the composition that is the subject of the present paper. This composition can also have the pyroxmangite structure. Maresch and Mottana (1976) determined the rhodonite + pyroxmangite equilibrium at 3–30 kbar H_2O pressure and extrapolated the curve to 1 bar, ~670 K. Pyroxmangite is the low-temperature form. Nevertheless, Huebner (1986) found that mixtures of SiO_2 (quartz or silica glass) and $MnCO_3$ or $Mn_{1-x}O$ in H_2O (1–2 kbar) invariably crystallized as pyroxmangite at <1123 K. Rhodonite was obtained only if the reaction was conducted in fused $MnCl_2 \cdot 4H_2O$ at pressure.

Previous measurements of the thermodynamic properties of $MnSiO_3$ were made by Kelley (1941), who measured C_P^0 at 27 temperatures between 52.6 and 294.8 K. Kelley's sample was prepared by dry sintering of a mixture of precipitated $MnCO_3$ and silica in a Ni cartridge heated to 1323 K for 5 d under flowing H gas. We presume that the sample crystallized as rhodonite, rather than pyroxmangite. Southard and Moore (1942) determined the heat content, $H_T^0 - H_{298}^0$, of this same sample of $MnSiO_3$ between 488.5 and 1508.7 K. King (1952) determined the enthalpy of the reaction

$$MnO + SiO_2 = MnSiO_3 \quad (1)$$

at 298.15 K (25 °C) by HF_{aq} solution calorimetry also using Kelley's sample. Other studies are summarized in Table 1.

The compositions of the braunite minerals are related to the composition of bixbyite, $(Mn > Fe)_8^{3+}O_{12}$, by means of the substitutions $Mn^{2+} + Si^{4+} \rightleftharpoons 2(Mn^{3+},Fe^{3+})$ to form

TABLE 1. Enthalpy of formation of $MnSiO_3$ calculated from various sources of calorimetric and equilibrium measurements

Type of measurement	Enthalpy $\Delta_f H^0_{298.15}$ (kJ/mol)	Reference
HF_{aq} solution calorimetry	−1319.4	King (1952); Hemingway and Robie (1977)
Activity-composition relations in Fe-Mn-Si-O at 1423 K	−1324.5	Schwerdtfeger and Muan (1966)
Activity-composition relations in Co-Mn-Si-O at 1473 K	−1327.7	Biggers and Muan (1967)
$MnCO_3 + SiO_2 = MnSiO_3 + CO_2$ at 2000 bars CO_2, 781 K	−1324.0	Peters (1971)
$MnCO_3 + SiO_2 = MnSiO_3 + CO_2$ at 500 bars CO_2, 746 K	−1318.2	Candia et al. (1975)
Molten salt calorimetry in $2PbO \cdot B_2O_3$ at 986 K	−1320.8	Navrotsky and Coons (1976)
$MnCO_3 + SiO_2 = MnSiO_3 + CO_2$ at 1000 bars CO_2, 758 K	−1321.2	Abrecht (1988)
$MnO + SiO_2 = MnSiO_3$ emf at 950–1300 K	−1323.1	Rog and Pycior (1987)

braunite, $Mn^{2+}Mn_6SiO_{12}$, and $Ca^{2+} + Si^{4+} \rightleftharpoons 2(Mn^{3+},Fe^{3+})$ to form braunite II, $Ca_{0.5}Mn_7Si_{0.5}O_{12}$, and neltnerite, $CaMn_6SiO_{12}$. Most samples of natural braunite and neltnerite have nearly "end-member" compositions (with 10% SiO_2 and either 0 or 9% CaO by weight), indicating that either of these substitutions can be dominant. However, plots of the compositions of some braunite define an irregular field extending toward neltnerite and braunite II (Baudracco-Gritti, 1985), indicating that both substitutions can occur simultaneously. Additional substitutions in braunite are minor Mg^{2+}, Fe^{3+}, and Al^{3+} for Mn^{3+} (Bhattacharya et al., 1984; Baudracco-Gritti, 1985). The ratio (Mn + Ca + Mg)/Si is insensitive to the compositions of the coexisting minerals or peak metamorphic grade. Abs-Wurmbach et al. (1983) analyzed 24 samples of braunite from a wide range of metamorphic grades; the minimum and maximum SiO_2 concentrations were 9.50 and 11.08 wt% (0.96 and 1.09 Si cations per eight-cation formula unit). Similarly, Bhattacharya et al. (1984) present 19 braunite analyses; the range in SiO_2 was 9.25–10.41 wt% (0.93–1.04 Si cations per 12-O formula unit). Thus, the Si content of ideal braunite, $Mn^{2+}Mn_6SiO_{12}$, should be a good approximation to that of naturally occurring braunite.

Early laboratory investigations of phase equilibria in the system $MnO-SiO_2-O_2$ indicated that "Mn_2O_3" could accommodate from 0 to at least 40 wt% SiO_2 and that a single phase containing at least 40 wt% SiO_2 could be synthesized at 1367–1493 K from quenched Mn-Si-O melt (Muan, 1959a, 1959b). Muan proposed that the operative substitution was Si^{4+} for Mn^{4+} in $Mn^{2+}Mn^{4+}O_3$ and that the observed limit of ≥40 wt% SiO_2 supported the presence of Mn^{4+}. In a brief subsequent report (Ito, 1961), bementite [$Mn_8Si_6O_{15}(OH)_{10}$] was said to oxidize at low temperatures to SiO_2-rich braunite. Thus, the seemingly variant composition of natural braunite with 10% SiO_2 by weight (neltnerite and braunite II were not yet known) was surprising. The early experimental results were not confirmed by Abs-Wurmbach (1980), who was unable to synthesize braunite with Mn/Si > 7/1 or < 6.8/1.2, corresponding to $Mn^{2+}_{1.0-1.2}Mn^{3+}_{6.0-5.6}Si_{1.0-1.2}O_{12}$. More Mn-rich compositions in the system $MnO-SiO_2-O_2$ yielded braunite and either bixbyite (1073 K) or hausmannite (≥1288 K); more siliceous compositions yielded braunite and silica or a pyroxenoid. Dasgupta et al. (1986) performed experiments in the system $MnO-FeO-SiO_2-O_2$. Microprobe analyses of Fe-bearing braunite from nine different experiments had 0.797–1.125 Si cations per formula unit, averaging 0.994 Si, close to the ideal value. Because the Si content does not correlate with the presence of quartz or jacobsite, the range is probably experimental error. Recently, de Villiers and Buseck (1989) predicted the occurrence of 21 polysomes, having 0–10 wt% SiO_2, in the bixbyite-braunite group. In addition to bixbyite, braunite II, and neltnerite, they observed three new polysomes, using high-resolution transmission electron microscopy methods. Their work suggests that there may be many ordered states having compositions between the now familiar species bixbyite, braunite, braunite II, and neltnerite. Although their results provide an explanation for the observed 0–10 wt% range in the SiO_2 contents of the braunite-group minerals, there is neither experimental confirmation nor a modern structural explanation for the reported SiO_2 contents of braunite that exceed 10% by weight.

Petrogenetic (T-f_{O_2}) grids for the system Mn-Si-C-O containing braunite were first presented by Huebner (1967), who noted that Si-rich and Si-poor braunite compositions led to topologically distinct multibundles of invariant points. Si-rich braunite samples plot on the Si-rich side of the join $Mn_2SiO_4-O_2$ in the subsystem $MnO-SiO_2-O_2$. The invariant point experimentally delineated by Muan (1959b) involves Si-rich braunite and results in the coexistence of braunite and tephroite (Mn_2SiO_4) (Fig. 1A). Chemographic analysis indicates that a vapor-absent (condensed) reaction with suggested braunite stoichiometry $Mn^{2+}_3Mn^{3+}_3Si_3O_{12} + Mn_2SiO_4 = 4MnSiO_3 + Mn_3O_4$, not shown by Muan, must originate at the invariant point. The equilibria of Muan (1959b) that are relevant to the present work are the reactions of tephroite + vapor to form rhodonite + hausmannite and of rhodonite + hausmannite + vapor to form braunite.

Compositions of Si-poor braunite plot on the Mn-rich side of the tephroite-vapor join; the multibundle for silica-poor braunite (Fig. 1B), in which braunite cannot be in equilibrium with tephroite, is consistent with natural assemblages. Huebner (1967, 1976) incorporated this multibundle in a petrogenetic grid for the system Mn-Si-O-C. This grid was modified by Peters et al. (1974) and Abs-Wurmbach et al. (1983). Dasgupta and Manickavasagam (1981) added Fe to the grid. Despite these refinements, great uncertainties still surround the placement of braunite equilibria in T-f_{O_2} space.

Sample preparation

The preparation of the sample of rhodonite used for our measurements was described by Robie et al. (1989). The rhodonite crystals are transparent, brownish red to rose pink, and have well developed faces. Rhodonite X-ray diffraction patterns were recorded with a Guinier-Hagg camera, using Cr$K\alpha$ radiation and Si standard; preliminary unit cell dimensions were reported in Robie et al. (1989). Following remeasurement of the films, all observed diffraction lines were indexed by comparison with a powder pattern calculated from the structure of Peacor and Niizeki (1963) but using the formula unit $Mn_5Si_5O_{15}$. The results are given in Table 2. Electron microprobe analysis of our crystals yielded MnO = 54.52 ± 0.2 wt% and SiO_2 = 46.14 ± 0.45 wt%. These values are the average and standard deviation based on 19 analyses. This composition corresponds to the formula unit $Mn_{1.00}Si_{1.00}O_3$. The probe standards used were synthetic Mn_2SiO_4 for Mn and Kakanui hornblende for Si, Al, Ca, and Fe (see Huebner and Woodruff, 1985).

Braunite with Mn/Si = 7 is stable at relatively high f_{O_2} but decomposes if the temperature exceeds about 1433 K in air (Muan, 1959a; Abs-Wurmbach, 1980; Abs-Wurmbach et al., 1983). We prepared braunite from a mix of analyzed-reagent-grade MnO_2 (Baker lot no. 30740) and silica glass (Corning no. 7904) that had been used previously by Robie and Hemingway (1985) and by Huebner (1986). A 50 g mix was ground and heated ten times in air in a large, initially covered Pt dish, for a total of 2417 h at an average temperature of 1298 K. After the second heating, the cover was removed to promote reaction (see Abs-Wurmbach, 1980). Reaction progress was monitored by examining the experiment products in immersion oil and by using X-ray powder diffraction patterns [particularly the intensities of the (624) and (123) reflections of braunite, compared with the (400) and (122) reflections of hausmannite]. The proportion of braunite increased, and that of hausmannite decreased, systematically with time. Virtually no isotropic glass, or weakly anisotropic cristobalite or tridymite, was detected. Only in the early stages could a possible silica phase be resolved by X-ray diffraction: a very weak, poorly defined peak in the position of the (101) reflection of cristobalite. Strong hausmannite and braunite reflections together with a weak silica peak might indicate initial formation of Si-rich braunite. At no stage was any other phase detected. If we were to synthesize braunite in the future, we would use cristobalite rather than silica glass, so that the silica phase might be better monitored with X-ray diffraction. The final product consisted of braunite and $\ll$0.1% by volume hausmannite (under crossed nicols, minute grains of the highly anisotropic, brilliantly orange to red grains of hausmannite are clearly discernable against the braunite).

The X-ray powder diffractometer peaks were exceedingly sharp. Unit cell dimensions were determined using a combination of 11 small splits of braunite and Si [a = 5.4307(2) Å] or BaF_2 [a = 6.1971(1) Å] as internal standards, using digital methods (Huebner, 1986). Each reflection was indexed by comparison with the calculated pattern of Smith and Anderson (1979), which showed good agreement with our observed intensities, and refined using the program of Evans et al. (1963). Each data set was processed a second time, using relaxed criteria for peak resolution (so that more, and possibly insignificant,

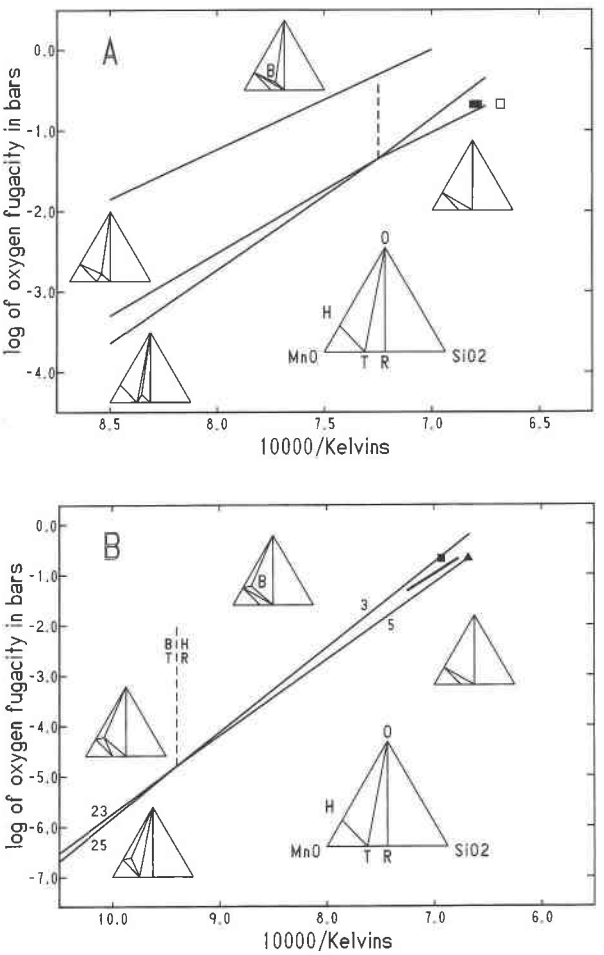

Fig. 1. Topology about invariant points involving the phases braunite (B), hausmannite (H), rhodonite (R), tephroite (T), and vapor (V) in the system MnO-SiO_2-O_2 at 1 bar total pressure. Lines are calculated from the thermodynamic properties listed in Table 10; dashed lines are metastable (vapor-absent) reactions. (**A**) Topology involving Si-rich braunite with reactions as positioned by Muan (1959b). The reaction of rhodonite + vapor to form Si-rich braunite + silica is shown even though it is not involved with the invariant point. Also shown are new experiments (this paper) bracketing Reaction 5. (**B**) Topology involving Si-poor braunite, following the results presented in this paper. The heavy solid line corresponds to Muan's (1959b) determination of Reaction 5, $2Mn_3O_4 + 6MnSiO_3 = 6Mn_2SiO_4 + O_2$. Symbols represent bracketing experiments from Table 4. The metastable extensions of Reactions 4 and 6 would fall outside of the region bounded by Reactions 23 and 25, were the extensions to be shown.

TABLE 2. Unit cell parameters and molar volumes of synthetic rhodonite and pyroxmangite forms of $MnSiO_3$ and of braunite, Mn_7SiO_{12}

a (Å)	*b* (Å)	*c* (Å)	α (°)	β (°)	γ (°)	cell *V* (Å³)	mol *V* (cm³)	References
				Rhodonite				
7.62	11.84	6.70	92.67	94.40	105.5	579	34.87	Ito (1972)
7.627(2)	11.853(3)	6.709(1)	92.47(2)	94.42(2)	105.70(2)	580.9(2)	34.98(1)	Momoi (1974)
7.616(3)	11.851(5)	6.707(2)	92.55(10)	94.35(10)	105.67(10)	579.8(5)	34.92(3)	Narita et al. (1977)
7.614(3)	11.856(6)	6.703(2)	92.40(4)	94.25(4)	105.73(4)	579.6(3)	34.91(1)	Huebner (1986)
7.620(1)	11.852(2)	6.704(1)	92.48(2)	94.38(1)	105.65(1)	580.0(1)	34.93(1)	Huebner (1986)
7.624(2)	11.852(4)	6.710(1)	92.32	94.47	105.68	580.8(3)	34.98(2)	Abrecht (1988)
7.616(1)	11.853(2)	6.706(1)	92.44(2)	94.40(2)	105.70(1)	579.8(1)	34.92(1)	Robie et al. (1989)
7.613(2)	11.849(2)	6.701(1)	92.49(2)	94.36(2)	105.64(2)	579.1(1)	34.87(1)	(42 refl., Si std)
7.615(2)	11.857(3)	6.703(1)	92.46(3)	94.45(2)	105.62(2)	579.8(2)	34.92(1)	(32 refl., Si std)
7.610(4)	11.845(5)	6.697(2)	92.52(4)	94.31(5)	105.56(4)	578.6(3)	34.84(2)	(27 refl., Si std)
				Pyroxmangite				
6.722(2)	7.600(2)	17.461(5)	113.80(2)	82.27(2)	94.77(2)	808.2(4)	34.76(2)	Momoi (1974)
6.717(2)	7.603(1)	17.448(5)	113.83(2)	82.35(3)	94.72(2)	807.5(3)	34.74(1)	Maresch and Mottana (1976)
6.721(2)	7.603(3)	17.455(6)	113.17(10)	82.27(10)	94.13(10)	812.4(8)	34.95(3)	Narita et al. (1977)
6.717(2)	7.601(2)	17.429(11)	113.79(3)	82.35(5)	94.73(3)	806.5(5)	34.70(2)	Huebner (1986), expt. 67
6.718(1)	7.598(1)	17.469(7)	113.80(2)	82.28(3)	94.68(2)	808.1(3)	34.76(1)	Huebner (1986), expt. 130
6.718(1)	7.598(1)	17.469(7)	113.80(2)	82.28(3)	94.68(2)	808.1(4)	34.76(2)	Huebner (1986)
6.707(3)	7.594(2)	17.405(11)	113.38	82.43	94.65	804.4(6)	34.60(3)	Abrecht (1988)
6.711(3)	7.582(4)	17.417(12)	113.74(5)	82.27(8)	94.69(5)	803.5(6)	34.55(3)	Peters (1971), reindexed
				Braunite				
9.4267(3)		18.6995(18)				1661.7(2)	125.09(2)	(25 refl., BaF_2 std.)
9.4261(4)		18.6986(16)				1661.4(2)	125.06(2)	(35 refl., BaF_2 std.)
9.4269(6)		18.6982(16)				1661.6(2)	125.08(2)	(25 refl., Si std.)
9.4262(5)		18.7046(22)				1661.2(2)	125.05(2)	(42 refl., Si std.)
9.428(1)		18.701(2)				1662.3(3)	125.13(2)	Abs-Wurmbach (1980)
9.4248(2)*		18.6989(9)				1661.0(1)	125.03(8)	de Villiers (1980)
9.44(0.05)*		18.76(1)				1671.8(15)	125.84(11)	de Villiers and Herbstein (1967)
9.432(2)*		18.703(7)				1663.9(8)	125.25(6)	de Villiers (1975)
9.408(16)*		18.668(32)				1652.3(49)	124.37(37)	Moore and Araki (1976)

* Naturally occurring material.

maxima in the data could be resolved) with the result that more peaks could be indexed and were accepted in the refinement, but that the overall quality of the least-squares fit was reduced slightly (Table 2). There is no evidence (such as peak broadening or additional reflections) for a phase with other than an ordered 18.699(1) Å repeat distance.

To gage the level of contamination in the laboratory, we obtained instrumental neutron activation analyses (see Baedecker and McKown, 1987) and some semiquantitative, DC-arc emission spectrographic (see Golightly et al., 1987) analyses of the reagents and synthesis products (Table 3). The only significant impurities detected in the reagents were about 500 ppm Ca in the MnO_2 and increases in Cr and Fe following crushing (in a hardened steel mortar) and acid leaching of the SiO_2 glass. For comparison, typical analyses of uncontaminated SiO_2 (Hetherington and Bell, 1967) reveal Cl (10–100 ppm), Ti (0.1–10 ppm), and Fe (0.01–5 ppm), and all other elements (<1 ppm each). Replicate INAA analyses of the braunite reveal that Fe and Cr increased by 240 and 400 ppm, respectively, probably from the furnace windings, and that Ir increased 41 ppm, probably from the Pt-ware crucible. Splits of the rhodonite sample, taken after calorimetric measurements, showed no evidence of contamination during synthesis; the 140 ppb Au is probably from the calorimeter.

In Table 2, we compare unit cell parameters for our calorimetric samples together with a number of recent values for synthetic rhodonite and pyroxmangite and for both synthetic and natural braunite. We did not include the values of Dasgupta et al. (1986) because their samples of synthetic braunite and pyroxmangite were ferruginous. The braunite and rhodonite unit cell parameters are in excellent agreement. Furthermore, the parameters for rhodonite prepared anhydrously by flux growth (Robie et al., 1989) and by hydrothermal synthesis (Huebner, 1986) agree excellently. As a best value for the molar volume of the ten samples of synthetic rhodonite we adopt 34.91 $\pm$ 0.05 cm³ and for the five samples of synthetic braunite 125.08 $\pm$ 0.03 cm³.

For pyroxmangite the agreement between reported investigations is not as good. The pyroxmangite cell dimension published by Peters (1971) is anomalously small (V = 779 Å³). Following reindexing of his pattern by comparison with a pattern calculated from the structure of Pinckney and Burnham (1988), but with composition $Mn_7Si_7O_{21}$, we could account for all observed lines. Revised dimensions based on 37 unambiguously indexed lines are reported in Table 2 and are now consistent with other reports. The cell dimension for experiment 130 in Table 2 is for the same material measured by Huebner (1986), but now 27 lines were refined, decreasing the standard errors. Based on the results summarized in Ta-

TABLE 3. Trace element analyses of reactants and products

	SiO_2*	SiO_2**	MnO_2†	Braunite‡	Rhodonite§
Na (ppm)	20	30	60	30	30
Ca‖		20	520		
Cr	0.3	39.0	6	243	8.6
Fe	20	200	30	370	40
Co	0.01	0.08	3.4	4.2	5.2
Ni	<1	<2	4	<17	10
Zn	0.4	0.6	5.3	9	2.4
Mo	<0.3	1.1	4.3	<6	0.7
Au	1.5	<0.5	3.2	12	140
Ir (ppb)	<0.4	<0.6	<0.3	41400	6.7

Note: Sc, As, Rb, Sb, Cs, Hf, Ta, Th, and U were analyzed and found to be <1 ppm each; K, Sr, Zr, and Ba were also analyzed and found to be below the detection limit, which exceeds 1 ppm. REE below the limit detection or <1 ppm, whichever is greater.

* Lumps from broken disk of SiO_2 glass.

** SiO_2 glass from same disk, crushed to pass 100 mesh and acid leached.

† MnO_2, reagent grade (Baker lot no. 30740).

‡ Braunite synthesized from SiO_2** and MnO_2† in Pt-ware dish open to furnace. Average of two analyses.

§ Rhodonite synthesized from SiO_2** and MnO_2†.

‖ Semiquantitative DC-arc emission spectroscopy.

TABLE 4. Results of experiments in air

Reactants	T (°C)	T (K)	t (h)	Products*	Stable
1	1025	1298	771	BCR	B
1	1050	1323	263	RBC	?
1	1075	1348	991	BRC	?
1	1100	1373	263	R	R
1	1150	1423	263	R	R
2	1050	1323	261	BHR	B
2	1100	1373	261	BHR	B
2	1150	1423	261	B(H)	B
2	1171	1444	171	BRH	B
2	1196	1469	656	HR	HR
2	1224	1497	354	HT	HT
3	1025	1298	771	BH(C?)	B
3	1050	1323	261	BH	?
3	1100	1373	261	BH(R?)	?
3	1150	1423	261	BH(R?)	?
3	1171	1444	171	BHR	BR
4	1196	1469	656	HR	HR
4	1201	1474	429	HR	HR
5	1201	1474	429	HR	HR

Note: 1 = braunite (B), cristobalite (C), and rhodonite (R) in the proportions of Eq. 2; 2 = braunite, hausmannite (H), and rhodonite in the proportions of Eq. 3; 3 = braunite, hausmannite, and cristobalite in the proportions of Eq. 4; 4 = hausmannite + tephroite (T) synthesized from Mix 2; 5 = braunite.

* In order of estimated abundance.

ble 2, the average value for the molar volume of the eight samples of synthetic pyroxmangite is 34.73 ± 0.12 cm^3. The volume change for the phase transition rhodonite $\rightleftharpoons$ pyroxmangite is -0.18 ± 0.13 cm^3 per mole of $MnSiO_3$. This change is consistent with pyroxmangite being the high-pressure, low-temperature polymorph of $MnSiO_3$.

PHASE EQUILIBRIUM EXPERIMENTS

Knowledge of the phase equilibria of reactions involving braunite, rhodonite, and other phases serves to (1) provide high-temperature free energies of reaction, which, when combined with the heat capacity (entropy) data, will yield free energies of formation of braunite and rhodonite as a function of temperature; and (2) provide some T-f_{O_2} values with which to position the high-temperature, high-f_{O_2} portion of the petrogenetic grid. The only previous attempt to locate reactions that bound the high-temperature, low f_{O_2} side of the braunite field is by Abs-Wurmbach et al. (1983). Although they emphasized the possible compositional range of braunite solid solution and braunite oxidation reactions, four unreversed experiments, in air, are relevant: rhodonite → braunite + cristobalite at 1288 K, braunite + quartz → rhodonite at 1436 and 1502 K, and braunite → rhodonite + hausmannite at 1459 K. These experiments deal with two reactions, shown on the grid of Huebner (1967, 1976, and to which the reader is specifically referred), that bound the high-temperature, low f_{O_2} side of the braunite stability field

$$2Mn_7SiO_{12} + 12SiO_2 = 14MnSiO_3 + 3O_2 \quad (2)$$

and, at higher temperatures,

$$2Mn_7SiO_{12} = 4Mn_3O_4 + 2MnSiO_3 + O_2. \quad (3)$$

On the basis of chemography, Huebner (1967, 1976) showed that these reactions should intersect such that, at lower f_{O_2} and temperatures, there would be only one reaction bounding the lower f_{O_2}, high-temperature side of the braunite field:

$$3Mn_7SiO_{12} = 7Mn_3O_4 + 3SiO_2 + O_2. \quad (4)$$

The metastable extension of Reaction 4 should lie subparallel to Reaction 3 and at lower f_{O_2} (higher temperature) values; if rhodonite failed to nucleate, we should be able to locate this reaction, even though metastable.

Cristobalite was synthesized by heating SiO_2 glass in a covered Pt crucible, contained in a high-purity alumina muffle tube, at 1788 K for 22 h. Synthetic hausmannite (Huebner and Sato, 1970) and rhodonite (Robie et al., 1989) have been described previously. Mixtures of reactants and products in the molar proportions specified by the reaction were heated in air. Reactants and products were identified by X-ray powder diffraction and oil-immersion methods to determine which phases grew at the expense of other phases. Results are tabulated in Table 4. Reaction 2 lies between 1298 and 1373 K. Reaction 3 lies between 1444 and 1469 K. We were not successful in locating Reaction 4. Using mixtures of braunite + hausmannite + rhodonite and of hausmannite + tephroite, we were also able to determine that the reaction

$$2Mn_3O_4 + 6MnSiO_3 = 6Mn_2SiO_4 + O_2 \quad (5)$$

lies between 1474 and 1497 K.

CALORIMETRIC MEASUREMENTS

The calorimeters and techniques used for measuring heat capacities from 5 to 1000 K in our laboratory have been described previously [see for example Robie (1987), Hemingway et al. (1981)]. Our experimental measure-

TABLE 5. Molar heat capacities of rhodonite* determined by adiabatic calorimeter

T (K)	Heat capacity [J/(mol·K)]	T (K)	Heat capacity [J/(mol·K)]	T (K)	Heat capacity [J/(mol·K)]
Series 1		**Series 3**		**Series 4** (cont.)	
301.65	87.63	59.34	20.97	239.96	76.63
306.50	88.51	64.38	22.87	245.28	77.50
311.83	89.46	69.44	23.63	250.64	78.53
317.16	90.89	74.77	25.09		
322.48	91.02	80.50	27.47	**Series 5**	
327.79	91.90	86.02	29.81		
333.05	93.08	91.59	32.28	255.78	79.54
338.31	93.91	97.20	34.64	261.64	80.61
343.59	94.75	102.68	36.88	267.13	81.64
348.91	95.24	108.06	39.01	272.64	82.75
354.23	95.69	113.36	41.06	278.13	83.65
		118.59	43.03	283.61	84.73
Series 2		123.74	44.97	289.07	85.86
		128.83	46.88	294.53	86.92
4.46	6.674	133.87	48.67	299.98	87.61
5.42	5.333	138.87	50.46	305.41	88.57
6.42	5.161	143.84	52.04	310.83	89.50
7.03	5.159	148.77	53.76		
7.83	5.205	153.68	55.09	**Series 6**	
8.78	5.437				
9.77	5.567	**Series 4**		51.37	15.56
10.77	5.553			55.07	17.91
11.74	5.668	150.30	54.42	58.56	20.76
13.09	5.538	155.75	55.98	62.27	22.11
14.82	5.540	160.84	57.46	66.36	23.51
16.57	5.611	165.96	59.00	70.30	23.90
18.72	5.520	170.77	60.32	74.13	25.06
21.14	5.524	175.55	61.69	77.84	26.56
23.51	5.674	180.35	62.91		
25.92	5.994	185.14	64.30	**Series 7**	
28.82	6.747	189.94	65.56		
32.19	7.468	194.76	66.74	51.50	15.64
35.67	8.578	199.59	67.94	53.54	16.86
39.74	10.57	204.45	69.09	55.50	18.23
44.34	11.97	209.34	70.31	57.52	20.42
49.01	14.12	214.28	71.31	59.70	20.64
		219.26	72.42	61.86	21.95
		224.32	73.45	63.97	22.92
		229.46	74.42	66.04	23.52
		234.68	75.54		

* Formula weight 131.022 g/mol.

TABLE 6. Molar heat capacities of braunite* determined by adiabatic calorimeter

T (K)	Heat capacity [J/(mol·K)]	T (K)	Heat capacity [J/(mol·K)]	T (K)	Heat capacity [J/(mol·K)]
Series 1		**Series 5**		**Series 7** (cont.)	
302.39	382.8	88.49	181.9	213.17	314.7
307.66	386.5	89.24	186.7	219.53	320.3
313.15	389.0	90.01	189.4	226.03	326.0
318.61	393.0	90.88	197.6	232.75	331.8
324.03	396.1	91.71	203.5	239.64	337.2
329.44	398.8	92.54	213.2	246.60	342.7
334.86	400.2	93.36	229.6	253.62	348.4
340.26	404.2	94.19	213.7	260.69	353.8
345.68	407.2	95.09	181.9	267.80	359.1
		95.97	180.3		
Series 2		96.77	180.3	**Series 8**	
		97.59	181.0		
38.74	37.15	98.43	180.1	275.03	364.4
43.16	46.39	99.27	180.6	282.30	368.9
		100.11	181.6	289.34	375.1
Series 3		100.95	182.5	296.40	379.1
		101.78	182.9	303.48	384.0
47.92	56.78				
52.86	68.50	**Series 6**		**Series 9**	
57.21	79.59				
62.07	92.37	97.01	180.4	5.20	0.6279
67.37	107.0	101.95	182.9	5.37	0.3846
72.36	121.9	106.89	188.6	5.49	0.3686
		111.88	194.6	5.76	0.5700
Series 4		116.75	200.6	6.05	0.6029
		121.64	207.2	6.64	0.9568
77.30	137.4	126.48	213.8	7.20	1.149
81.76	152.8	131.28	220.1	8.15	1.946
86.03	170.5	136.04	226.4	9.39	2.447
90.54	195.9	140.78	232.4	10.61	2.973
95.05	197.2	145.50	238.3	11.85	3.587
99.76	181.2	150.20	244.8	12.96	4.327
104.36	185.7	154.88	250.1	14.25	5.115
108.59	190.8	159.55	255.7	15.80	6.178
		164.22	261.2	17.49	7.457
				19.38	9.122
		Series 7		21.50	11.12
				23.87	13.61
		169.68	267.6	26.53	16.78
		175.93	275.3	29.51	20.86
		182.13	282.0	32.87	26.18
		188.40	289.7	36.61	33.75
		194.50	295.9	40.80	41.68
		200.68	302.3	45.41	50.99
		206.89	308.4	50.36	62.22

* Formula weight 604.644 g/mol.

ments are listed in Tables 5, 6, and 7 in their chronological order of measurement.

The heat capacity of rhodonite was measured between 5 and 354 K. The mass of the calorimetric sample was 16.834 g. The contribution of the sample to the total measured heat capacity ranged from 97% at 5.4 K to a minimum of 20% at 80 K. Although we had anticipated finding a λ-peak in C_P^0 at low temperatures, none was observed. However, in the temperature range 5–30 K, C_P^0 was essentially constant with a value of approximately 5.4 J/(mol·K), as shown in Figure 2. The magnetic susceptibility of $MnSiO_3$ was measured between 4.2 and 300 K by Sawaoka et al. (1968), who report a Néel temperature of 7 K. Our C_P^0 data suggest that if $MnSiO_3$ orders antiferromagnetically it must do so at a temperature below 6 K.

The heat capacity of braunite (Mn_7SiO_{12}) was measured by adiabatic calorimetry between 5.2 and 345.6 K. Braunite exhibits a λ-point in C_P^0 with a Néel temperature (i.e., paramagnetic to antiferromagnetic transition temperature, T_N) between 93.4 and 94.2 K, in good agreement with Abs-Wurmbach et al. (1981), who reported 93 K on the basis of the magnetic susceptibility of synthetic powdered braunite. The heat capacity of braunite between 75 and 110 K is shown in Figure 3. The braunite sample had a mass of 43.923 g and ranged from 71 to 40% of the measured total heat capacity. The heat capacity of braunite was also measured between 340 and 900 K by differential scanning calorimetry. For these measurements the sample mass was 21.041 mg, the heating rate was 10 K/min, and the sensitivity was 0.0084 J/s.

We are unaware of any previous calorimetric measure-

TABLE 7. Differential scanning calorimeter measurements of braunite

T (K)	C_p^0 [J/(mol·K)]	T (K)	C_p^0 [J/(mol·K)]
338.7	400.1	459.4	449.7
348.8	406.0	469.5	451.1
358.8	410.6	479.6	453.5
368.9	415.7	489.6	454.0
379.0	420.0	499.7	455.7
389.0	424.4	509.7	458.8
399.1	428.3	519.8	459.2
409.1	432.4	529.9	461.3
419.2	435.7	599.3	476.0
429.3	439.1	699.9	492.2
439.3	442.7	800.5	506.3
449.4	445.9	899.5	521.2

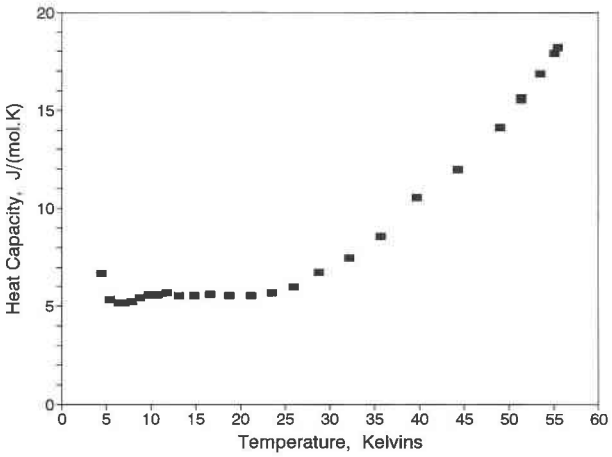

Fig. 2. Molar heat capacity C_p^0 of synthetic rhodonite ($MnSiO_3$) between 5 and 55 K. Note the absence of a pronounced λ transition.

ments on braunite. Miyano and Beukes (1987) estimated values for C_p^0, S_{298}^0, and $\Delta_f H_{298}^0$ of braunite.

Bennington et al. (1987) reported C_p^0 data for two natural manganese silicates, pyroxmangite of composition $(Mn_{0.93}Ca_{0.056}Mg_{0.01}Fe_{0.010})SiO_3$ from Butte, Montana, and zincian rhodonite of composition $(Mn_{0.632}Ca_{0.21}Zn_{0.09}Mg_{0.05}Fe_{0.02})SiO_3$ from Franklin, New Jersey. They reported a λ-like transition in C_p^0 of pyroxmangite at −272.1 K and Schottky anomalies in the heat capacities of pyroxmangite and zincian rhodonite at 11 and 8 K, respectively. The temperature of the λ-like transition in their pyroxmangite coupled with the large amount (0.37 wt%) of H_2O+ in the analysis strongly suggests that the cause of the peak in C_p^0 at 272.1 K is due to the melting of ice in fluid inclusions in the pyroxmangite and is not a property of $MnSiO_3$. Furthermore, neither our sample of rhodonite nor the $MnSiO_3$ of Kelley (1941), both of which were synthesized anhydrously, nor the zincian rhodonite sample of Bennington et al. (1987), which has only 0.02 wt% H_2O+, exhibits the transition that the pyroxmangite shows. We believe this transition is due to the enthalpy of fusion of ice. This phenomenon has been observed previously in materials that contain significant numbers of fluid inclusions, e.g., euclase (Hemingway et al., 1986).

The absence of a λ-peak in C_p^0 of rhodonite is somewhat surprising for such a magnetically concentrated compound. A large-scale plot of the C_p^0 data of Bennington et al. (1987) for pyroxmangite and zincian rhodonite, of Kelley's (1941) values for synthetic $MnSiO_3$, and our own flux-grown synthetic rhodonite, all reduced to the same mass, shows systematic differences. Below approximately 130 K our values and those of Kelley (1941) are always greater than those for pyroxmangite and very much greater than those for the zincian rhodonite sample, and the percentage difference increases with decreasing temperature. We believe that this is a reflection of the replacement of the paramagnetic Mn^{2+} by diamagnetic Ca and Zn ions in the natural mineral samples, and, further, that this implies that the magnetic contribution of the Mn^{2+} ion to the heat capacity is still significant at temperatures of the order of 100 K. Note that approximately 6 and 35% of the Mn^{2+} has been replaced by diamagnetic ions in the pyroxmangite and zincian rhodonite samples of Bennington et al. (1987), respectively, and, furthermore, that both samples contain appreciable amounts of Fe^{2+}.

The crystal structure of rhodonite has been refined by Peacor and Niizeki (1963), by Ohashi and Finger (1976), and by Narita et al. (1977). The SiO_2 tetrahedra form zigzag chains with a repeat unit of five tetrahedra (fünferketten) separated by bands of edge-linked Mn coordination polyhedra. The important feature of the structure is that the ten Mn^{2+} of the unit cell ($Z = 10$) occupy five different equipoints. The M1, M2, and M3 Mn are coordinated by fairly regular octahedra, whereas M4 is fourfold–fivefold coordinated and M5 is sevenfold coordinated. This irregularity in the coordination polyhedra may be the reason that $MnSiO_3$ does not exhibit a sharp λ-transition above 6 K as do Mn_2SiO_4 (T_N = 47.4 K: Robie et al., 1982) or $MnCO_3$ (T_N = 34.3 K: Robie et al., 1984). Antiferromagnetic ordering of the Mn^{2+} presumably takes place by the superexchange mechanism (see, for example, White and Geballe, 1979), and this is sensitive to both the interionic spacing and to the cation-anion angle (Mn^{2+}-O^{2-}-Mn^{2+}), which is presumably different for each pair because of the nonequivalence of the Mn^{2+} equipoints.

The observed behavior of C_p^0 could arise from the persistence of short-range magnetic order above a cooperative magnetic transition at some temperature below our lowest measurement. A neutron diffraction study of the spin structures of rhodonite and pyroxmangite at He temperatures (4.2 K) and also of their magnetic susceptibilities at temperatures below 20 K would be most helpful for understanding the cause of the anomalous behavior of C_p^0 of rhodonite below 20 K.

THERMODYNAMIC PROPERTIES OF RHODONITE AND BRAUNITE

The low-temperature C_p^0 measurements were extrapolated to 0 K using the customary plot of C_p^0/T against

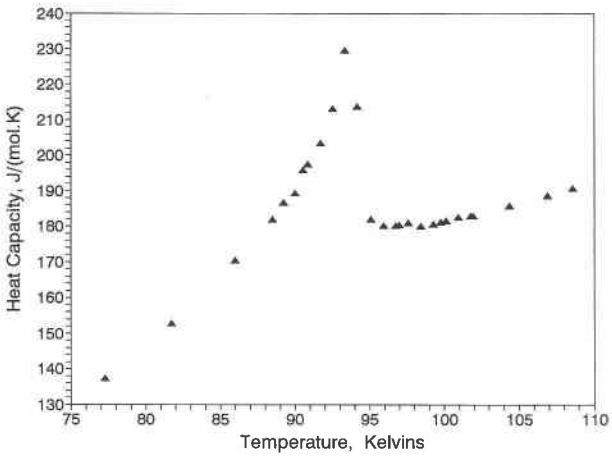

Fig. 3. Molar heat capacity C_P^0 of braunite (Mn_7SiO_{12}) between 75 and 110 K, showing the λ transition at a Néel temperature of 94 K. This point is associated with the antiferromagnetic-paramagnetic transition (discussed in text).

T^2. For braunite the entropy arising from this extrapolation is only 0.4 J/(mol·K). This value may be slightly low. Westerholt et al. (1986) observed a maximum in the magnetic susceptibility of braunite at 1 K. The process yielding this maximum could also cause a heat capacity anomaly and increase in entropy. For rhodonite, however, the very large values for C_P^0 at the lowest measured temperatures give rise to a significant amount of entropy below 6 K and accordingly increase the uncertainty in $S^0_{298.15}$ considerably.

Tables of the thermodynamic properties at integral temperatures were obtained by spline smoothing of the experimental C_P^0 data. Properties for rhodonite and braunite are listed in Tables 8 and 9, respectively.

The entropies at 298.15 K derived from our low-temperature measurements are 100.5 ± 1.0 and 416.4 ± 0.8 J/(mol·K) for rhodonite and braunite, respectively. Our C_P^0 data for rhodonite were combined with the high-temperature relative enthalpy data of Southard and Moore (1942) to generate values for C_P^0 up to 1500 K. For braunite we extrapolated our combined adiabatic and DSC measurements (6–900 K) graphically to 1500 K and generated a three-term Maier-Kelley equation to represent C_P^0 between 300 and 1500 K. The equation C_P^0 (braunite) $= 4.301 \times 10^2 + 1.110 \times 10^{-1} \times T - 7.325 \times 10^6/T^2$ fits the observed (300–900 K) data to 0.9%.

The available data for the enthalpy of formation of $MnSiO_3$ (rhodonite) are summarized in Table 1. There are two direct calorimetric measurements of the enthalpy change for Reaction 1. King (1952) used aqueous HF solution calorimetry at 298.15 K, whereas Navrotsky and Coons (1976) used the molten salt technique at 986 K. The equilibrium

$$MnCO_3 + SiO_2 = MnSiO_3 + CO_2 \qquad (6)$$

has been studied by Peters (1971), Candia et al. (1975), and Abrecht (1988). Their data were combined with the thermal functions for $MnCO_3$ of Robie et al. (1984), for MnO, CO_2, and SiO_2 of Robie et al. (1978), and f_{CO_2} calculated using the program of Kerrick and Jacobs (1981), to generate enthalpies for Reaction 6 at 298.15 K.

Schwerdtfeger and Muan (1966) give $\Delta_r G^0_{1423} = -24.68 \pm 1.26$ kJ for Reaction 1 based upon the extrapolation of their activity measurements on $(Mn,Fe)SiO_3$ to the pure Mn end-member. Biggers and Muan (1967) obtained $\Delta_r G^0_{1473} = -27.20$ kJ for this reaction on the basis of activity measurements for $(Mn,Co)SiO_3$ and $(Mn,Co)_2SiO_4$, extant values for $\Delta_f G^0_{1473}$ for $CoSiO_3$ and Co_2SiO_4, and the equilibrium

$$CoSiO_3 + MnSi_{0.5}O_2 = MnSiO_3 + CoSi_{0.5}O_2. \qquad (7)$$

Both of these investigations were made in the temperature region where the deviation of MnO from exact stoichiometry becomes significant. We used the values listed in Robie et al. (1978) for MnO and SiO_2 to convert these to $\Delta_r G^0_{298.15}$ and to $\Delta_f G^0$ ($MnSiO_3$, 298.15 K) assuming that the SiO_2 in both high temperature studies was tridy-

Table 8. Standard molar thermodynamic properties of rhodonite,* $MnSiO_3$

T (K)	Heat capacity C_P^0	Entropy $S_T^0 - S_0^0$	Enthalpy function $(H_T^0 - H_0^0)/T$	Gibbs energy function $-(G_T^0 - H_0^0)/T$
10	5.49	6.49	3.72	2.78
20	5.68	10.37	4.66	6.77
30	6.98	12.80	5.12	7.68
40	10.16	15.20	5.94	9.26
50	14.91	17.93	7.21	10.72
60	18.21	20.85	8.69	12.16
70	22.58	23.99	10.36	13.62
80	26.96	27.29	12.16	15.12
90	31.24	30.71	14.05	16.67
100	35.41	34.22	15.97	18.24
110	39.43	37.78	17.93	19.86
120	43.28	41.38	19.88	21.50
130	46.96	44.99	21.82	23.17
140	50.46	48.60	23.74	24.86
150	53.76	52.20	25.64	26.56
160	56.87	55.77	27.49	28.27
170	59.80	59.30	29.31	30.00
180	62.58	62.80	31.08	31.72
190	65.21	66.26	32.81	33.45
200	67.70	69.66	34.49	35.17
210	70.08	73.02	36.13	36.90
220	72.33	76.34	37.72	38.61
230	74.48	79.60	39.27	40.33
240	76.53	82.81	40.78	42.03
250	78.48	85.98	42.25	43.72
260	80.35	89.09	43.68	45.41
270	82.15	92.16	45.07	47.08
280	83.89	95.18	46.43	48.75
290	85.58	98.15	47.75	50.40
300	87.23	101.1	49.04	52.04
310	88.86	104.0	50.30	53.67
320	90.46	106.8	51.53	55.29
330	92.03	109.6	52.73	56.89
340	93.59	112.4	53.91	58.48
350	95.13	115.1	55.07	60.06
273.15	82.70	93.11	45.51	47.61
298.15	86.93	100.5	48.80	51.74

Note: units are joules per mole kelvin.
* Formula weight 131.022 g/mol.

mite, but because these compounds depart from system MnO-SiO_2-O_2 composition (Table 1), we excluded these values when generating Table 10.

Rog and Pycior (1987) obtained the Gibbs free energy change for the reactions

$$MnO + MnSiO_3 = Mn_2SiO_4 \quad (8)$$

and

$$Mn_2SiO_4 + SiO_2 = 2MnSiO_3 \quad (9)$$

using solid-electrolyte galvanic cells with manganese-β-alumina as the electrolyte, between 950 and 1300 K. Adding their $\Delta_r G^\circ$ values for Reactions 8 and 9 yields -27.21 ± 1.22 kJ for $\Delta_r G^\circ$ of Reaction 1, at the intermediate temperature, 1150 K. Using our thermal functions to reduce this to $\Delta_f H^\circ(MnSiO_3, 298.15\ K)$ gives -1323.1 ± 1.6 kJ/mol. Rog and Pycior's (1987) values show a drift of ≈ 0.5 kJ in the calculated value of $\Delta_r H^\circ(298.15\ K)$ as a function of measurement temperature (1000–1300 K). We can also use Rog and Pycior's (1987) data to calculate the Gibbs free energy change for the reaction

$$2MnO + SiO_2 = Mn_2SiO_4 \quad (10)$$

since $2\Delta_r G^\circ(\text{Reaction 8}) + \Delta_r G^\circ(\text{Reaction 9}) = \Delta_r G^\circ(\text{Reaction 10})$. This calculation yields -47.92 ± 1.95 kJ (at 1000 K) which is 3.6 kJ more negative than the value adopted by Robie et al. (1982). Unfortunately, the $\Delta_f G^\circ$ values for $MnSiO_3$ and Mn_2SiO_4 obtained from Rog and Pycior's (1987) data are not independent of one another inasmuch as both Reactions 8 and 9 involve $MnSiO_3$ and Mn_2SiO_4. At best we can say that the emf measurements are not in serious disagreement with our selected values. The slope of Rog and Pycior's (1987) $\Delta G^\circ(T)$ for Reaction 9 is -8.2 J/K whereas that calculated from the calorimetric entropy data is -6.4 J/K. Similarly, for Reaction 10 the slope obtained from the emf measurements is 4.0 J/K whereas that from the calorimetric entropies is 7.0 J/K. If we exclude the two high-temperature activity studies the average for $\Delta_f H^\circ(MnSiO_3, 298.15\ K)$ is -1321.6 ± 2.0 kJ/mol, which we adopt. This yields $\Delta_f G^\circ(MnSiO_3, 298.15\ K) = -1244.7 \pm 2.0$ kJ/mol.

The value which we have adopted for braunite, -4260 kJ/mol, was obtained by attempting simultaneously to satisfy our experimental brackets for Reaction 3, while also requiring the curves for Reactions 3 and 5 to intersect within the field outlined by Reactions 24, 6, and 17 (described below) as suggested by the absence of natural assemblages in which braunite coexists with tephroite and as required by the resulting chemography. We assumed that $\Delta_f H^\circ(Mn_7SiO_{12}, 298.15\ K)$ was the only variable quantity, i.e., the entropy changes for Reactions 3, 5, 6, 17, and 24, and the enthalpies of formation of all other phases (listed in Table 10) were exact. If we use -4260 kJ/mol as the enthalpy of formation of braunite together with the ancillary data from Table 10 we get T_{eq} for Reaction 3 of ≈ 1415 K at $f_{O_2} = 0.21$ bar (i.e., air), which is 24 K less than the lowest temperature allowed by our experimental brackets. The $\Delta_r S^\circ(298.15\ K)$ for Reaction 3 has an uncertainty of ± 2.7 J/K, and accordingly within the uncertainty in the entropy change we could have adjusted $\Delta_f H^\circ(298.15\ K)$ of braunite, as derived from the single equilibrium bracket at ≈ 1440 K, by ± 3.8 kJ/mol. Similarly, the uncertainty in $\Delta_r S^\circ$ of Reaction 5 is ± 6.5 J/K, and therefore the position of the intersection of Reactions 3 and 5 is only poorly constrained. The very limited amount of equilibrium data involving braunite, coupled with the fact that the data are all at the same f_{O_2}, make unwarranted any attempt to adjust the thermodynamic data of any of the other phases in the two reactions. Until more extensive temperature-dependent equilibrium data for Reaction 3 are available, we believe that -4260.0 ± 3.8 kJ/mol is the current best value for the enthalpy of formation of braunite at 298.15 K. Combining this value with our entropy we calculate $\Delta_f G^\circ(Mn_7SiO_{12}, 298.15\ K) = -3944.7 \pm 3.8$ kJ/mol. An error in the equilibrium temperature of 10 K corresponds

TABLE 9. Standard molar thermodynamic properties of braunite,* Mn_7SiO_{12}

T (K)	Heat capacity C_P°	Entropy $S_T^\circ - S_0^\circ$	Enthalpy function $(H_T^\circ - H_0^\circ)/T$	Gibbs energy function $-(G_T^\circ - H_0^\circ)/T$
5	0.39	0.124	0.092	0.032
10	2.70	0.984	0.734	0.250
15	5.67	2.60	1.85	0.75
20	9.72	4.76	3.29	1.47
25	14.91	7.46	5.07	2.39
30	21.57	10.74	7.24	3.50
35	30.38	14.69	9.88	4.81
40	40.16	19.40	13.06	6.34
45	50.23	24.70	16.62	8.08
50	61.50	30.56	20.54	10.02
60	86.85	43.98	29.44	14.54
70	114.6	59.41	39.59	19.82
80	147.0	76.75	50.91	25.84
90	188.7	96.38	63.83	32.55
93	222.4	103.04	68.30	34.72
100	181.4	116.8	76.82	40.01
110	193.1	134.7	86.85	47.85
120	205.4	152.0	96.21	55.79
130	218.2	168.9	105.1	63.81
140	231.1	185.6	113.6	72.0
150	243.9	201.9	121.9	80.0
160	256.3	218.1	129.9	88.2
170	268.3	234.0	137.7	96.3
180	279.8	249.6	145.3	104.3
190	290.9	265.1	152.7	112.4
200	301.4	280.3	159.8	120.5
210	311.3	295.2	166.8	128.4
220	320.6	309.9	173.6	136.3
230	329.4	324.4	180.2	144.2
240	337.7	338.6	186.6	152.0
250	345.7	352.5	192.8	159.7
260	353.3	366.2	198.8	167.4
270	360.7	379.7	204.7	175.0
280	367.8	392.9	210.4	182.5
290	374.7	406.0	215.9	190.1
300	381.3	418.8	221.3	197.5
310	387.9	431.4	226.6	204.8
273.15	363.0	383.9	206.5	177.4
298.15	380.1	416.4	220.3	196.1

Note: units are joules per mole kelvin.
* Formula weight 604.644 g/mol.

TABLE 10. Summary of thermodynamic properties of phases in the MnO-SiO_2-CO_2-O_2 system

Name and formula	Formula weight (g)	Entropy S^0_{298} [J/(mol·K)]	Enthalpy $\Delta_f H^0_{298}$ (kJ/mol)	Molar V^* (J/bar)	A1	A2	A3	A4	A5	Range (K)	Reference
Braunite	604.644	416.4	−4260.0	12.508	430.1	0.111	−7325000			298	This study
Mn_7SiO_{12}		0.8	3.8	0.005						1700	
Rhodonite	131.022	100.5	−1321.6	3.494	99.04	0.01915	−3041000	274.5		298	This study
$MnSiO_3$		1.0	2.0	0.005						1500	
Pyroxmangite	131.022	99.4	−1322.3	3.472						298	This study
$MnSiO_3$		2.0	3.0	0.002							
Pyrolusite	86.937	52.8	−520.0	1.661	290.4	−0.1442	2012000	−3787.0	4.541×10^{-5}	298	Robie and Hemingway (1985)
MnO_2		0.1	0.7	0.002						850	
Hausmannite	228.812	164.1	−1384.5	4.695	−7.432	0.09487	−6712000	3396.0		298	Robie and Hemingway (1985)
Mn_3O_4		0.2	1.4	0.006						1400	Keller et al. (1991)
Bixbyite	157.874	113.7	−959.0	3.137	162.4	0.01211	1046000	−1317.0	3.462×10^{-6}	325	Robie and Hemingway (1985)
Mn_2O_3		0.2	1.0	0.005						1400	
Tephroite	201.96	155.9	−1731.5	4.861	261.3	−0.01378		−22178.0		298	Robie et al. (1982)
Mn_2SiO_4		0.4	2.9	0.007						1600	
Manganosite	70.937	59.7	−385.2	1.322	60.28	0.0351	0	97.5		298	Robie et al. (1978)
MnO		0.4	0.5	0.0004						1800	
Rhodochrosite	114.947	98.0	−892.9	3.107	149.7	0.01876	141700	−1314.2		298	Robie et al. (1984)
$MnCO_3$		0.1	1.2	0.001						600	This study
Quartz	60.085	41.46	−910.7	2.2688	81.14	0.01828	−181000	−698.5	5.406×10^{-6}	298	Hemingway (1987)
SiO_2		0.16	1.0	0.0001						844	
Carbon dioxide**	44.01	213.79	−393.5	2478.97	88.11	−0.002698	723200	−1007.0		298	Garvin et al. (1987)
CO_2 (ideal gas)		0.04	0.2	0.02						2200	
Oxygen	31.999	205.15	0.0	2478.97	56.58	−0.005255	685600	−578.0	1.113×10^{-6}	298	Garvin et al. (1987)
O_2 (ideal gas)		0.0		0.02						2500	

Note: uncertainties as 2σ. $C^0_p = A1 + A2 \times T + A3/T^2 + A4/T^{0.5} + A5 \times T^2$.
* At standard temperature and pressure.
** The effect of pressure can be calculated from Kerrick and Jacobs (1981).

to a change in the derived value of $\Delta_f H^0(Mn_7SiO_{12}, 298.15\ K)$ of 1.1 kJ/mol.

Our measured value for $S^0_{298.15}$ of Mn_7SiO_{12} is 10.4 J/(mol·K) less than the estimated value of Miyano and Beukes (1987), and our value for $\Delta_f H^0(Mn_7SiO_{12}, 298.15\ K)$ is 24.0 kJ/mol more negative than their estimate. Their value for braunite was based in part upon phase equilibrium studies by Muan (1959b), which, as noted above, pertain to Si-rich braunite and which Abs-Wurmbach et al. (1983) did not reproduce.

Entropy and free energy of pyroxmangite

If we accept the slope of the phase boundary for the rhodonite = pyroxmangite transformation given by Maresch and Mottana (1976), ≈ 50 bar/K, our value for the entropy of rhodonite, and the previously derived difference in molar volumes, then we can calculate an entropy for pyroxmangite at 298.15 K of 99.0–99.5 J/(mol·K). Bennington et al. (1987) give 99.5 ± 0.2 J/(mol·K) for the entropy of pyroxmangite of supposed composition $(Mn_{0.955}Ca_{0.045})SiO_3$. Bennington et al. (1987) also give −1324.8 ± 4.2 kJ/mol for $\Delta_f H^0$(298.15 K) of pyroxmangite after correcting their results to the composition $MnSiO_3$. Furthermore, Navrotsky and Coons (1976) have measured the enthalpy change for the pyroxmangite-rhodonite transition by molten salt calorimetry with the result $\Delta_r H^0_{986} = 0.25 \pm 1.38$ kJ. All this is by way of emphasizing that the difference in the molar Gibbs free energies of pyroxmangite and rhodonite is quite small, of the order of 1 kJ/mol.

Mn-Si-O-C phase diagram

For convenience, we have assembled the thermodynamic data for the more important phases in the MnO-SiO_2-CO_2-O_2 system in Table 10. The values for the enthalpies of formation of the manganese oxides were taken from Robie and Hemingway (1985) except for Mn_3O_4, which was modified by the inclusion of the data of Keller et al. (1991), and the elimination of a typographic error (inversion of the last two digits) in the value for $\Delta_f H^0(Mn_3O_4, 298.15\ K)$ of Robie and Hemingway (1985).

These values were entered into a spreadsheet to calculate the equilibrium constants, as a function of temperature and pressure, for the reactions indicated below. The $RT \ln(f_{CO_2})$ term for those equilibria involving CO_2 was calculated using the f_{CO_2} polynomial given by Holland and Powell (1990). The results of the calculations for these reactions helped us develop Figure 4 and are

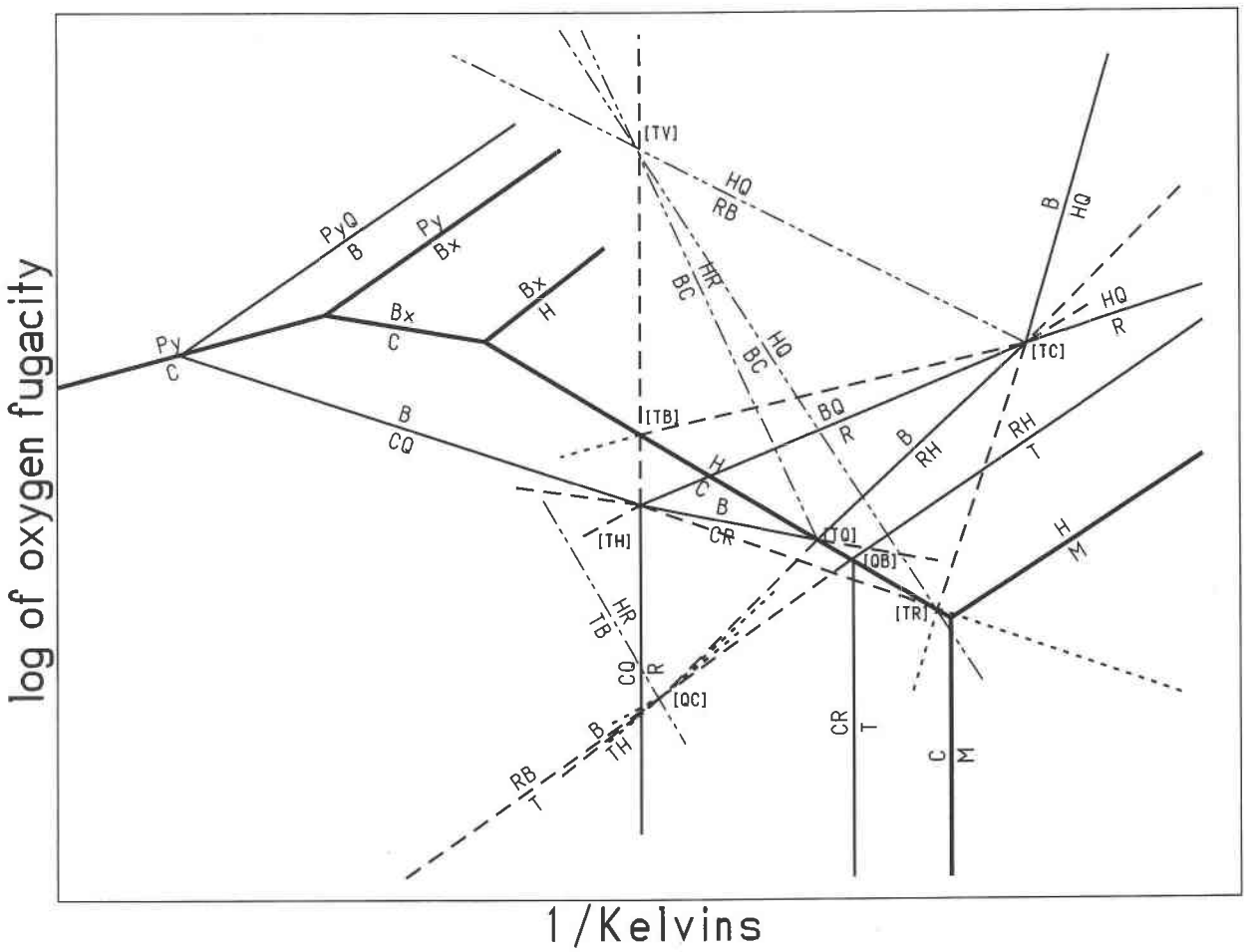

Fig. 4. Partial net of Schreinemakers bundles for the system MnO-SiO_2-C-O_2, not drawn to scale in order to show topologic relationships. Pressure greater than the vapor pressures of the solid phases; vapor is present and $P_t = P_{CO_2} + P_{CO} + P_{O_2}$. Phases are Py = pyrolusite (MnO_2), Bx = bixbyite (Mn_2O_3), M = manganosite ($Mn_{1-x}O$), C = rhodochrosite ($MnCO_3$), H = hausmannite, Q = quartz, B = braunite of nominal composition Mn_7SiO_{12}, R = Ca-free rhodonite, T = tephroite, and V = vapor. For simplicity, V is omitted when labeling reactions. Heavy solid lines represent stable reactions in the system Mn-C-O (Huebner, 1969). All other reactions are a consequence of adding SiO_2 to the system; those pertaining to the phases C, H, B, R, T, Q, and V are shown. Light solid lines are stable; dashed and dotted lines are metastable. Dash-dot-dot lines are condensed (vapor absent); although they cannot exist, they are shown for completeness. Invariant points are labeled by enclosing the two missing phases in brackets; [TR], [QC], and [TB] are metastable; [TV] is condensed.

summarized in Figure 5 as a plot of log f_{O_2} against $1/T$ (K) at 2 kbar total pressure. The reactions corresponding to the phase boundaries in Figure 5 are:

$$2Mn_7SiO_{12} + 12SiO_2 = 14MnSiO_3 + 3O_2 \quad (2)$$

$$2Mn_7SiO_{12} = 4Mn_3O_4 + 2MnSiO_3 + O_2 \quad (3)$$

$$3Mn_7SiO_{12} = 7Mn_3O_4 + 3SiO_2 + O_2 \quad (4)$$

$$2Mn_3O_4 + 6MnSiO_3 = 6Mn_2SiO_4 + O_2 \quad (5)$$

$$MnCO_3 + SiO_2 = MnSiO_3 + CO_2 \quad (6)$$

$$4Mn_3O_4 + O_2 = 6Mn_2O_3 \quad (11)$$

$$2Mn_2O_3 + O_2 = 4MnO_2 \quad (12)$$

$$MnCO_3 = MnO + CO_2 \quad (13)$$

$$6MnCO_3 + O_2 = 2Mn_3O_4 + 6CO_2 \quad (14)$$

$$4MnCO_3 + O_2 = 2Mn_2O_3 + 4CO_2 \quad (15)$$

$$2MnCO_3 + O_2 = 2MnO_2 + 2CO_2 \quad (16)$$

$$MnCO_3 + MnSiO_3 = Mn_2SiO_4 + CO_2 \quad (17)$$

$$2Mn_3O_4 + 6SiO_2 = 6MnSiO_3 + O_2 \quad (18)$$

$$6MnO + O_2 = 2Mn_3O_4 \quad (19)$$

$$14Mn_2O_3 + 4SiO_2 = 4Mn_7SiO_{12} + O_2 \quad (20)$$

$$14MnCO_3 + 2SiO_2 + 3O_2 = 2Mn_7SiO_{12} + 14CO_2 \quad (21)$$

$$7MnO_2 + SiO_2 = Mn_7SiO_{12} + 2O_2 \quad (22)$$

$$10MnSiO_3 + 2Mn_7SiO_{12} = 12Mn_2SiO_4 + 3O_2 \quad (23)$$

$$2Mn_7SiO_{12} + 12CO_2 = 12MnCO_3 + 2MnSiO_3 + 3O_2 \quad (24)$$

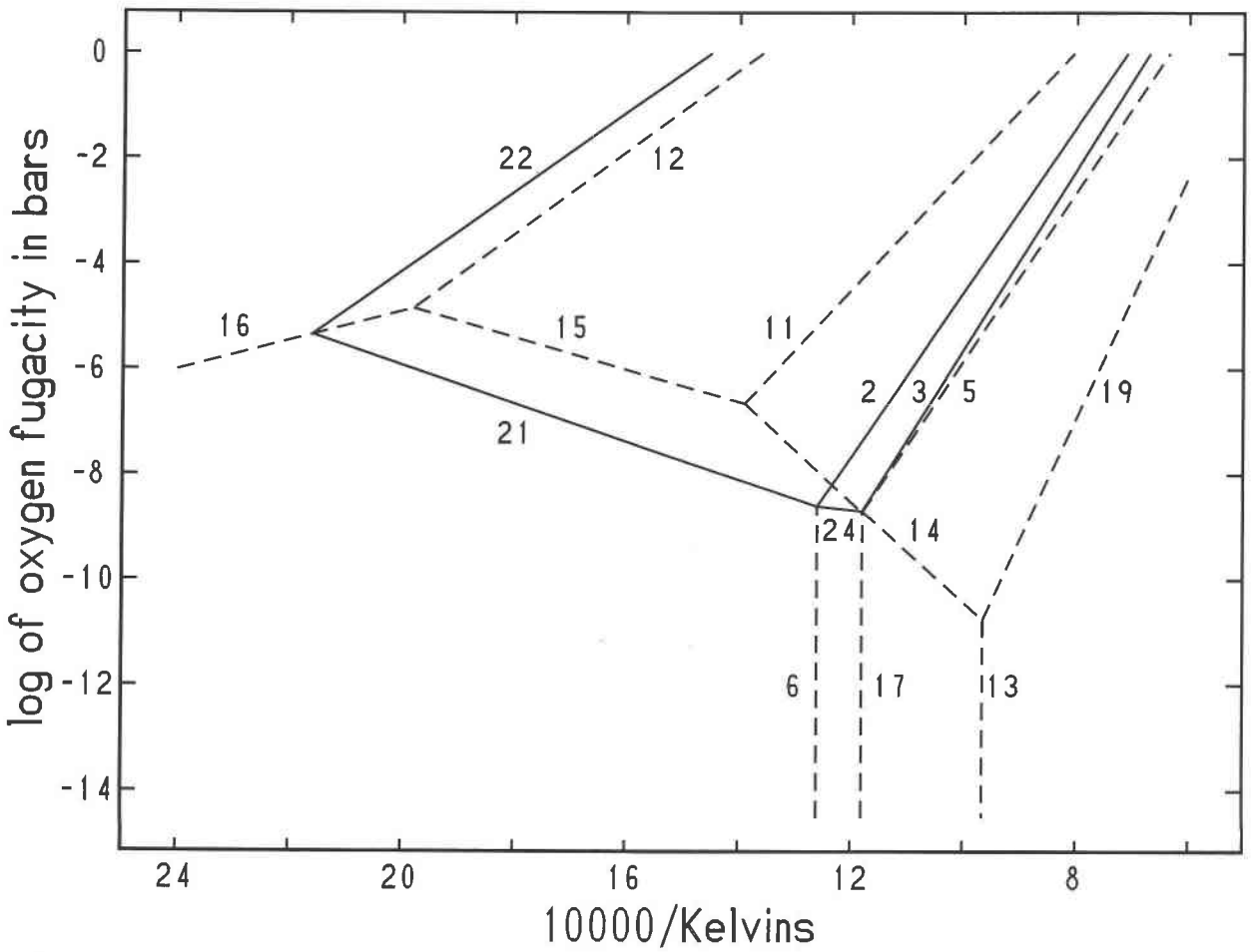

Fig. 5. Net of stable reactions at 2000 bars (0.2 GPa) calculated from the data of Table 10 and emphasizing reactions involving braunite. $P_t = P_{CO_2} + P_{CO} + P_{O_2}$ and the vapor is CO_2-rich in the temperature-log f_{O_2} region shown. Numbered reactions correspond to equations in text. Solid lines correspond to reactions involving braunite. Invariant points [TQ], [QB], and [QC], shown on Fig. 4, cannot be distinguished on this figure so six stable reactions (3, 5, 14, 17, 24, and 14) appear to radiate from a point.

$$3Mn_7SiO_{12} = 3Mn_2SiO_4 + 5Mn_3O_4 + 2O_2. \quad (25)$$

The stoichiometric coefficients for several of the phases, e.g., Mn_2O_3, $MnCO_3$, $MnSiO_3$, and SiO_2, are large, specifically in Reactions 20, 21, and 3; and inasmuch as the estimated uncertainties in $\Delta_f G^0$ for these phases are ± 1–2 kJ/mol, the effect upon the position of the calculated equilibrium arising from these uncertainties can be significant. For example, a change of 1 kJ/mol in $\Delta_f H^0(MnCO_3, 298.15\ K)$ would change the position of Reaction 21 by 0.49 in log f_{O_2}.

Many of these reactions are shown in Figure 4. The topology of the grid is derived from the petrogenetic grid presented by Huebner (1967, 1976), and the similar grid of Peters et al. (1974), but with two modifications arising from our new thermodynamic data for braunite (summarized in Table 10 and Fig. 5). (1) Reaction 21, CQ = B, by which rhodochrosite + quartz form braunite, now lies at lower f_{O_2} values. One consequence of this shift is that braunite oxidizes to pyrolusite + quartz (Reaction 22, B = PyQ) rather than to bixbyite + quartz (Reaction 20). This change is in accord with the aforementioned critical assemblage braunite + pyrolusite + quartz but precludes the critical assemblage braunite + bixbyite + quartz. Perhaps solid solution of Fe in braunite lowers the f_{O_2} at which braunite oxidizes, so that Fe-rich braunite oxidizes to Fe-rich bixbyite + quartz (similar to Reaction 20), and Fe-poor braunite oxidizes to pyrolusite + quartz (Reaction 22). A second consequence of the shifting of Reaction 21 is to make the reaction of rhodochrosite + rhodonite to form braunite stable (Reaction 24, CR = B). The critical natural assemblage rhodochrosite + rhodonite + braunite is unknown to us. (2) Invariant points [T,C] and [Q,C] have been modified (such that the stable extensions of the univariant curves have become metastable, and vice versa) and repositioned such that Reaction 2, R = BQ, lies at higher f_{O_2} than Reaction 3, RH = B, and these reactions diverge toward lower f_{O_2} and temperature, as required by Table 10 and Figure 5.

(As mentioned earlier, the enthalpy of braunite was also adjusted, within the limits of uncertainty, to satisfy the chemography.) The invariant point [Q,C] is now metastable and lies concealed by one of the fields in which carbonate is stable. The result of these changes is that Reactions 3, RH = B, and 5, T = RH now converge as temperature and f_{O_2} are decreased, consistent with the enthalpies of reaction. When the grid is positioned quantitatively and at the scale of Figure 5 in log f_{O_2} − $1/T$ (K) space at 2000 bars with vapor consisting predominantly of CO_2, invariant points [TQ], [QB], and [QC] appear to lie on top of each other.

Several features of Figures 4 and 5 merit comment. We are dealing with an isobaric four component system, Mn-Si-O-C; in the absence of graphite, we need only consider the compositional domain MnO-SiO_2-O_2-CO_2. According to the phase rule, an isobaric invariant point has five phases in equilibrium, and an isobaric univariant curve has four phases in equilibrium. Because the grid is an isobaric section with pressure fixed at greater than the vapor pressures of the solids, vapor-absent invariant points, univariant curves, and divariant fields cannot exist. Nevertheless, we show [TV] and its vapor-absent univariant curves for completeness.

In the the seven-phase subsystem rhodochrosite–Si-poor braunite–hausmannite–tephroite–Ca-free rhodonite–quartz–vapor, we show eight (of 21 possible) isobaric invariant points; of these eight, four are stable. The phases TRQ are compositionally colinear and there are two sets of coplanar phases, TQRV and CTRQ. The isobaric univariant curve HCV passes stably through isobaric invariant points [TB], [TQ], [QB], and [TR]; colinearities also occur along RCQV and RHBV. Reactions CHV and RVBQ cross indifferently because the compositional domains of these reactions do not overlap (CHV is silica-free). We know of no precedent for a systematic analysis of a system with four components, seven (or more) phases, and compositional degeneracy. We hope that the availability of consistent thermodynamic data for these phases may stimulate others in a systematic topological analysis.

Acknowledgments

We appreciate the valuable contributions made by supportive U.S. Geological Survey colleagues. In particular, H.T. Evans, Jr., measured, indexed, and refined the rhodonite X-ray data to obtain the cell dimensions of our synthetic rhodonite reported in Table 2. We regard his indexing of the triclinic rhodonite patterns as definitive and place great confidence in the resulting molar volume. J.N. Grossman obtained the INAA analyses listed in Table 3. I. Abs-Wurmbach provided a helpful review.

References cited

Abrecht, J. (1988) Experimental evaluation of the $MnCO_3$ + SiO_2 = $MnSiO_3$ + CO_2 equilibrium at 1 kbar. American Mineralogist, 73, 1285–1291.

——— (1989) Manganiferous phyllosilicate assemblages: Occurrences, compositions, and phase relations in metamorphosed Mn deposits. Contributions to Mineralogy and Petrology, 103, 228–241.

Abs-Wurmbach, I. (1980) Miscibility and compatibility of braunite, $Mn^{2+}Mn_6^{3+}O_8/SiO_4$, in the system Mn-Si-O at 1 atm in air. Contributions to Mineralogy and Petrology, 71, 393–399.

Abs-Wurmbach, I., Hewat, A.W., and Sabine, T.M. (1981) Magnetische- und Neutronenbeugungs-Experimente an Braunit, $Mn^{2+}Mn_6^{3+}O_8/SiO_4$. Zeitschrift für Kristallographie, 154, 240–242.

Abs-Wurmbach, I., Peters, T., Langer, K., and Schreyer, W. (1983) Phase relations in the system Mn-Si-O: An experimental and petrological study. Neues Jahrbuch für Mineralogie Abhandlungen, 146, 258–279.

Baedecker, P.A., and McKown, D.M. (1987) Instrumental neutron activation analysis of geochemical samples. In P.A. Baedecker, Ed., Methods for geochemical analysis. U.S. Geological Survey Bulletin 1770, H1–H14.

Baudracco-Gritti, C. (1985) Substitution du manganee bivalent par du calcium dan les mineaux du groupe: Braunite, neltnérite, braunite II. Bulletin de Minéralogie, 108, 437–445.

Bennington, K.O., Brown, R.R., Bell, H.E., and Beyer, R.P. (1987) Thermodynamic properties of two manganese silicates, pyroxmangite and fowlerite. U.S. Bureau of Mines Report of Investigations, 9064, 22 p.

Bhattacharya, P.K., Dasgupta, S., Fukuoka, M., and Roy, S. (1984) Geochemistry of braunite and associated phases in metamorphosed non-calcareous manganese ores of India. Contributions to Mineralogy and Petrology, 87, 65–71.

Biggers, J.V., and Muan, A. (1967) Activity-composition relations in orthosilicate and metasilicate solid solutions in the system MnO-CoO-SiO_2. Journal of the American Ceramic Society, 50, 230–235.

Bonatti, E., Zerbi, M., Kay, R., and Rydell, H. (1976) Metalliferous deposits from the Apennine ophiolites: Mesozoic equivalents of modern deposits from oceanic spreading centers. Geological Society of America Bulletin, 87, 83–94.

Candia, M.A.F., Peters, T., and Valarelli, J.V. (1975) The experimental investigation of the reactions $MnCO_3$ + SiO_2 = $MnSiO_3$ + CO_2 and $MnSiO_3$ + $MnCO_3$ = Mn_2SiO_4 + CO_2 in CO_2/H_2O gas mixtures at a total pressure of 500 bars. Contributions to Mineralogy and Petrology, 52, 261–266.

Crerar, D.A., Namson, J., Chyi, M.S., Williams, L., and Feigenson, M.D. (1982) Manganiferous cherts of the Franciscan assemblage: I. General geology, ancient and modern analogues, and implications for hydrothermal convection at oceanic spreading centers. Economic Geology, 77, 519–540.

Dasgupta, H.C., and Manickavasagam, R.M. (1981) Regional metamorphism of non-calcareous manganiferous sediments from India and the related petrogenetic grid for a part of the system Mn-Fe-Si-O. Journal of Petrology, 22, 363–396.

Dasgupta, S., Banerjee, H., and Fukuoka, M. (1985) Oxidation gradients in metamorphosed non-carbonatic manganese formations. Contributions to Mineralogy and Petrology, 90, 258–261.

Dasgupta, S., Banerjee, H., Miura, H., and Hariya, Y. (1986) Stability of braunite and associated phases in parts of the system Mn-Fe-Si-O. Mining Geology, 36, 351–360.

Dasgupta, S., Banerjee, H., Fukuoka, M., Bhattacharya, P.K., and Roy, S. (1990) Petrogenesis of metamorphosed manganese deposits and the nature of the precursor sediments. Ore Geology Reviews, 5, 359–384.

de Villiers, J.P.R. (1975) The crystal structure of braunite with reference to its solid-solution behavior. American Mineralogist, 60, 1098–1104.

——— (1980) The crystal structure of braunite II and its relation to bixbyite and braunite. American Mineralogist, 65, 756–765.

de Villiers, J.P., and Buseck, P.R. (1989) Stacking variations and nonstoichiometry in the bixbyite-braunite polysomatic mineral group. American Mineralogist, 74, 1325–1336.

de Villiers, P.R., and Herbstein, F.H. (1967) Distinction between two members of the braunite group. American Mineralogist, 52, 20–30.

Evans, H.T., Jr., Appleman, D.E., and Handwerker, D.S. (1963) The least squares refinement of crystal unit cells with powder diffraction data by an automatic computer indexing method. American Crystallographic Association Annual Meeting Program, 42–43.

Flohr, M.J.K., and Huebner, J.S. (1992) Mineralogy and geochemistry of two sedimentary manganese deposits, Sierra Nevada, California. Lithos, 29, 57–85.

Garvin, D., Parker, V.B., and White, H.J., Jr., Eds. (1987) CODATA thermodynamic tables: Selections for some compounds of calcium and related mixtures: A prototype set of tables, 356 p. Hemisphere, Washington, DC.

Golightly, D.W., Dorrzapf, A.F., Jr., Mays, R.E., Fries, T.L., and Conklin,

N.M. (1987) Analysis of geologic materials by direct-current arc emission spectrography and spectrometry. In P.A. Baedecker, Ed., Methods for geochemical analysis. U.S. Geological Survey Bulletin 1770, A1–A13.

Hein, J.R., Koski, R.A., and Yeh, H.-W. (1987) Chert-hosted manganese deposits in sedimentary sequences of the Franciscan Complex, Diablo Range, California. In J.R. Hein, Ed., Siliceous sedimentary rock-hosted ores and petroleum, p. 206–230. Van Nostrand Reinhold, New York.

Hemingway, B.S. (1987) Quartz: Heat capacities from 340 to 1000 K and revised values for the thermodynamic properties. American Mineralogist, 72, 273–279.

Hemingway, B.S., and Robie, R.A. (1977) Enthalpies of formation of $(Al(OH)_3)$, and $NaAlO_2$: Revised values for $\Delta H^0_{f,298}$ and $\Delta G^0_{f,298}$ of some alumino-silicate minerals. Journal of Research of the U.S. Geological Survey, 5, 413–429.

Hemingway, B.S., Krupka, K.M., and Robie, R.A. (1981) Heat capacities of the alkali feldspars between 350 and 1000 K from differential scanning calorimetry, the thermodynamic functions of the alkali feldspars from 298.15 to 1400 K, and the reaction quartz + jadeite = analbite. American Mineralogist, 66, 1202–1215.

Hemingway, B.S., Barton, M.D., Robie, R.A., and Haselton, H.T., Jr. (1986) Heat capacities and thermodynamic functions for beryl, $Be_3Al_2Si_6O_{18}$, phenakite, Be_2SiO_4, euclase, $BeAlSiO_4(OH)$, bertrandite, $Be_4Si_2O_7(OH)_2$, and chrysoberyl, $BeAl_2O_4$. American Mineralogist, 71, 557–568.

Hetherington, G., and Bell, L.W. (1967) Analysis of high-purity synthetic vitreous silicas. Physics and Chemistry of Glasses, 8, 206–208.

Holland, T.J.B., and Powell, R. (1990) An enlarged and updated internally consistent thermodynamic data set with uncertainties and correlation: The system K_2O-Na_2O-CaO-MgO-MnO-FeO-Fe_2O_3-Al_2O_3-TiO_2-SiO_2-C-H_2-O_2. Journal of Metamorphic Petrology, 8, 89–124.

Huebner, J.S. (1967) Stability relations of minerals in the system Mn-Si-C-O, 279 p. Ph.D. thesis, Johns Hopkins University, Baltimore, Maryland.

——— (1969) Stability relations of rhodochrosite in the system manganese-carbon-oxygen. American Mineralogist, 54, 457–481.

——— (1976) The manganese oxides: A bibliographic commentary. In Mineralogical Society of America Reviews in Mineralogy, 3, SH1–SH17.

——— (1986) Nature of phases synthesized along the join $(Mg,Mn)_2Si_2O_6$. American Mineralogist, 71, 111–122.

Huebner, J.S., and Flohr, M.J.K. (1990) Microbanded manganese formations: Protoliths in the Franciscan Complex, California. U.S. Geological Survey Professional Paper 1502, 72 p.

Huebner, J.S., and Sato, M. (1970) The oxygen fugacity-temperature relationships of manganese oxide and nickel oxide buffers. American Mineralogist, 55, 934–952.

Huebner, J.S., and Woodruff, M.E. (1985) Chemical compositions and critical evaluation of microprobe standards available in the Reston microprobe facility. U.S. Geological Survey Open File Report 85-718, 276 p.

Huebner, J.S., Flohr, M.J.K., and Grossman, J.N. (1992) Chemical fluxes and origin of a manganese carbonate-oxide-silicate deposit in bedded chert. Chemical Geology, 100, 93–118.

Ito, J. (1972) Rhodonite-pyroxmangite peritectic along the join $MnSiO_3$-$MgSiO_3$ in air. American Mineralogist, 57, 865–876.

Ito, K. (1961) Thermal transformation of bementite (abs.). Journal of the Japanese Association of Mineralogists, Petrologists and Economic Geologists, 45, 209–218.

Keller, M., Xuae, J., and Dieckmann, R. (1991) Electrochemical investigation of the oxygen activity at the manganosite-hausmannite equilibrium. Journal of the Electrochemical Society, 138, 3398–3401.

Kelley, K.K. (1941) The specific heats at low temperatures of ferrous silicate, manganous silicate, and zirconium silicate. Journal of the American Chemical Society, 63, 2750–2752.

Kerrick, D.M., and Jacobs, G.K. (1981) A modified Redlich-Kwong equation for H_2O, CO_2, and H_2O-CO_2 mixtures at elevated pressures and temperatures. American Journal of Science, 281, 735–767.

King, E.G. (1952) Heats of formation of manganous metasilicate (rhodonite) and ferrous orthosilicate (fayalite). Journal of the American Chemical Society, 74, 4446–4448.

Maresch, W.V., and Mottana, A. (1976) The pyroxmangite-rhodonite transformation for the $MnSiO_3$ composition. Contributions to Mineralogy and Petrology, 55, 69–79.

Miyano, T., and Beukes, N.J. (1987) Physicochemical environments for the formation of quartz-free manganese oxide ores from the early Proterozoic Hotazel formation, Kalahari manganese field, South Africa. Economic Geology, 82, 706–718.

Momoi, H. (1974) Hydrothermal crystallization of $MnSiO_3$ polymorphs. Mineralogical Journal, 7, 359–373.

Moore, P.B., and Araki, T. (1976) Braunite: Its structure and relationship to bixbyite, and some insights on the genealogy of fluorite derivative structures. American Mineralogist, 61, 1226–1240.

Muan, A. (1959a) Phase equilibria in the system manganese oxide-SiO_2 in air. American Journal of Science, 257, 297–315.

——— (1959b) Stability relations among some manganese minerals. American Mineralogist, 44, 946–960.

Narita, H., Koto, K., and Morimoto, N. (1977) The crystal structure of $MnSiO_3$ polymorphs (rhodonite- and pyroxmangite-type). Mineralogical Journal, 8, 329–342.

Navrotsky, A., and Coons, W.E. (1976) Thermochemistry of some pyroxenes and related compounds. Geochimica et Cosmochimica Acta, 40, 1281–1288.

Nel, C.J., Beukes, N.J., and de Villiers, J.P.R. (1986) The Mamatwan manganese mine of the Kalahari manganese field. In C.R. Annaeusser and S. Maske, Eds., Mineral deposits of southern Africa, p. 963–987. Geological Society of South Africa, Johannesburg, South Africa.

Ohashi, Y., and Finger, L.W. (1976) Pyroxenoids: A comparison of the refined structures of rhodonite and pyroxmangite. Annual Report of the Director, Geophysical Laboratory, 564–569.

Ostwald, J., and Bolton, B.R. (1990) Diagenetic braunite in sedimentary rocks of the Proterozoic manganese group, Western Australia. Ore Geology Reviews, 5, 315–323.

Peacor, D.R., and Niizeki, N. (1963) The redetermination and refinement of the crystal structure of rhodonite, $(Mn,Ca)SiO_3$. Zeitschrift für Kristallographie, 119, 98–116.

Peters, T. (1971) Pyroxmangite: Stability in H_2O-CO_2 mixtures at a total pressure of 2000 bars. Contributions to Mineralogy and Petrology, 32, 267–273.

Peters, T., Schwander, H., and Trommsdorff, V. (1973) Assemblages among tephroite, pyroxmangite, rhodochrosite, quartz: Experimental data and occurrences in the Rhetic Alps. Contributions to Mineralogy and Petrology, 42, 325–332.

Peters, T., Valarelli, V., and Candia, M.A.F. (1974) Petrogenetic grids from experimental data in the system Mn-Si-C-O-H. Revista Brasileira Geociências, 4, 15–26.

Pinckney, L.R., and Burnham, C.W. (1988) High-temperature crystal structure of pyroxmangite. American Mineralogist, 73, 809–817.

Robie, R.A. (1987) Calorimetry. In G.C. Ulmer and H.L. Barnes, Eds., Hydrothermal experimental techniques, p. 389–422. Wiley-Interscience, New York.

Robie, R.A., and Hemingway, B.S. (1985) Low-temperature molar heat capacities and entropies of MnO_2 (pyrolusite), Mn_3O_4 (hausmannite), and Mn_2O_3 (bixbyite). Journal of Chemical Thermodynamics, 17, 165–181.

Robie, R.A., Hemingway, B.S., and Fisher, J.F. (1978) Thermodynamic properties of minerals and related substances at 298.15 K and 1 bar (10^5 Pascals) and at higher temperatures. U.S. Geological Survey Bulletin 1452, 456 p.

Robie, R.A., Hemingway, B.S., and Takei, H. (1982) Heat capacities and entropies of Mg_2SiO_4, Mn_2SiO_4, and Co_2SiO_4 between 5 and 380 K. American Mineralogist, 67, 470–482.

Robie, R.A., Haselton, H.T., Jr., and Hemingway, B.S. (1984) Heat capacities and entropies of rhodochrosite ($MnCO_3$) and siderite ($FeCO_3$) between 5 and 600 K. American Mineralogist, 69, 349–357.

Robie, R.A., Russell-Robinson, S., and Evans, H.T., Jr. (1989) Flux growth of $MnSiO_3$ (rhodonite) crystals. Journal of Crystal Growth, 94, 981–982.

Rog, G., and Pycior, W. (1987) Determination of the standard molar Gibbs free energies of formation of the manganese silicates by e.m.f. measurements. Journal of Chemical Thermodynamics, 19, 381–384.

Roy, S. (1965) Comparative study of the metamorphosed manganese protores of the world: The problem of the nomenclature of the gondites and kodurites. Economic Geology, 60, 1238–1260.

Roy, S., Dasgupta, S., Majumdar, N., Banerjee, H., Bhattacharya, P.K., and Fukuoka, M. (1986) Petrology of manganese silicate-carbonate-oxide rock of Sausar Group, India. Neues Jahrbuch für Mineralogie Monatshefte, 12, 561–568.

Sawaoka, A., Miyahara, S., and Akimoto, S.I. (1968) Magnetic properties of several metasilicates and metagermanates with pyroxene structure. Journal of the Physical Society of Japan, 25, 1253–1257.

Schwerdtfeger, K., and Muan, A. (1966) Activities in olivine and pyroxenoid solid solutions of the system Fe-Mn-Si-O at 1150°C. Transactions of the Metallurgical Society of the AIME, 236, 201–211.

Smith, D., and Anderson (1979) JCPDS Grant-in-Aid-Report. Pennsylvania State University, University Park, Pennsylvania.

Southard, J.C., and Moore, G.E. (1942) High-temperature heat content of Mn_3O_4, $MnSiO_3$ and Mn_3C. Journal of the American Chemical Society, 64, 1769–1770.

Westerholt, K., Abs-Wurmbach, I., and Dahlbeck, R. (1986) Antiferromagnetism and spin-glass order in Fe-, Ca-, and Al-substituted braunites $Mn^{2+}(Mn^{3+})_6SiO_{12}$. Physical Review B, 34, 6437–6447.

White, R.M., and Geballe, T.H. (1979) Long range order in solids, 413 p. Academic, New York.

Manuscript received May 12, 1994
Manuscript accepted January 25, 1995